Chemical characteristics of brown carbon in atmospheric particles at a suburban site near Guangzhou, China

Yi Ming Qin[1,#], Hao Bo Tan[2], Yong Jie Li[3], Zhu Jie Li[2,4], Misha I. Schurman[5], Li Liu[2,6], Cheng Wu[7], and Chak Keung Chan[1]

[1]School of Energy and Environment, City University of Hong Kong, Hong Kong, China

[2]Key Laboratory of Regional Numerical Weather Prediction, Institute of Tropical and Marine Meteorology, China Meteorological Administration, Guangzhou, China

[3]Department of Civil and Environmental Engineering, Faculty of Science and Technology, University of Macau, Macau, China

[4]School of Environmental Science and Engineering, Nanjing University of Information Science and Technology, Nanjing, China

1 [5] Zephyr Research Consultants, USA

[6]Department of Atmospheric Science, Sun yat-sen University, Guangzhou, China

[7]Institute of Mass Spectrometer and Atmospheric Environment, Jinan University, Guangzhou, China

[#] now at School of Engineering and Applied Sciences, Harvard University, Cambridge, MA, USA

Correspondence to: Chak K. Chan (chak.k.chan@cityu.edu.hk) and Yong Jie Li (yongjieli@umac.mo)

Abstract:

Light-absorbing organic carbon (or brown carbon, BrC) in atmospheric particles has received much attention for its potential role in global radiative forcing. While a number of field measurement campaigns have differentiated light absorption by black carbon (BC) and BrC, the chemical characteristics of BrC are not well understood. In this study, we present co-located real-time light absorption and chemical composition measurements of atmospheric particles to explore the relationship between the chemical and optical characteristics of BrC at a suburban site downwind of Guangzhou, China from November to December 2014. BrC and BC contributions to light absorption were estimated using measurements from a seven-wavelength aethalometer, while the chemical composition of non-refractory PM_1 was measured with a high resolution time-of-flight aerosol mass spectrometer (HR-ToF-AMS). Using the Absorption Angstrom Exponent (AAE) method, we estimated that BrC contributed 23.6% to the total aerosol absorption at 370 nm, 18.1% at 470 nm, 10.7% at 520 nm, 10.7% at 590 nm, and 10.5% at 660 nm. Biomass burning organic aerosol (BBOA) has the highest mass absorption coefficient among sources of organic aerosols. Its contribution to total brown carbon absorption coefficient decreased but that of low-volatility oxygenated organic aerosol (LVOOA) increased with increasing wavelength, suggesting the need for wavelength-dependent light absorption analysis for BrC in association with its chemical makeup. Clear correlations of N-containing ion fragments with absorption coefficient were observed. These correlations also depended on their degrees of unsaturation/cyclization and oxygenation. While the current study relates light absorption by BrC to ion fragments, more detailed chemical characterization is warranted to constrain this relationship.

Atmospheric
Chemistry
and Physics
Discussions

3 Introduction:

4 Atmospheric particles participate considerably in the global climate direct effect via their light-

5 scattering (e.g., sulfate) and/or light-absorbing components (e.g., black carbon, BC). BC is the

6 major contributor to light absorption that increases the atmospheric energy budget, but the

7 contribution of brown carbon (BrC) cannot be ignored. The BrC absorption contribution to total

8 aerosol forcing can reach 20–50% over regions dominated by seasonal biomass burning and

9 biofuel combustion (Feng et al., 2013). BrC absorbs light primarily at UV and short visible

10 wavelengths, absorbing negligible amounts at long visible wavelengths, while BC absorbs strongly

11 throughout the visible spectrum (Andreae and Gelencsér, 2006; Bergstrom et al., 2007; Bond and

12 Bergstrom, 2006). In global climate models, the direct radiative forcing of organic aerosols at the

13 top of atmosphere can shift from cooling (-0.08 Wm^{-2}) to warming ($+0.025$ Wm^{-2}) when strong

14 BrC absorption is included (Feng et al., 2013). However, uncertainties in the sources, formation,

15 chemical composition, and absorption properties of BrC hinder more accurate estimations of

16 radiative forcing induced by atmospheric particles.

17 BrC is operationally defined and has many chemical constituents, which makes chemical

18 characterization quite challenging. Both primary and secondary organic aerosols can act as BrC

19 (Laskin et al., 2015). For example, biomass burning organic aerosol (BBOA) has been identified

20 as a contributor to BrC in rural areas in the southern United States (Di Lorenzo et al., 2017;

21 Washenfelder et al., 2015), while coal combustion organic aerosol (CCOA) contributes

22 substantially to BrC during winter in Beijing (Yan et al., 2017). Species from secondary formation

23 processes, such as humic-like substances (HULIS) formed by in-cloud processing (Rinco et al.,

24 2009), species from gas-phase photo-oxidation of volatile organic compounds (VOCs) in the

25 presence of NO_x, and species from reactions between carbonyl compounds and ammonia in the

26 aqueous film at the particle surface, can also contribute to BrC (Gen et al., 2018; Laskin et al.,

27 2010; Liu et al., 2015). Highly conjugated organics, nitro-aromatic compounds, imidazoles, and

28 other N-heterocyclic compounds have been found in BrC (Laskin et al., 2015; Lin et al., 2016).

29 Sun et al. (2007) also found that light-absorbing organic molecules in BrC are likely large (i.e.,

30 possessing > 18 carbon atoms); these molecules are generally highly unsaturated and contain three

31 or more oxygen atoms and/or one or more nitrogen atoms.

32 The Pearl River Delta (PRD) region, one of the most economically developed regions in China,

33 suffers under air pollution from a variety of sources (Chan and Yao, 2008; Li et al., 2017). Source

Atmospheric
Chemistry
and Physics
Discussions

34   apportionment using positive matrix factorization (PMF) analysis of mass spectral data sets from

35   high resolution time-of-flight aerosol mass spectrometry (HR-ToF-AMS) has revealed that the

36   organic aerosol (OA) in this region arises from traffic emissions (i.e., hydrocarbon-like organic

37   aerosol, or HOA), biomass burning (BBOA), cooking (COA), and secondary formation (i.e.,

38   oxygenated organic aerosols, or OOAs). In the PRD, HOA is often the largest contributor to OA

39   at urban sites (He et al., 2011), while SOA plays a more important role at rural sites (Gong et al.,

40   2012; Huang et al., 2011). BBOA has also been found to contribute significantly to total OA in the

41   PRD region, with contributions of 24% at an urban site in Shenzhen (He et al., 2011) and 14% and

42   25% at rural sites in Heshan and Kaiping, respectively (Gong et al., 2012; Huang et al., 2011).

43   Yuan et al. (2016) attributed 6-12% of the total aerosol absorption at 405 nm at a rural site in the

44   PRD to BrC; the authors found higher BrC contributions during fall, which they ascribed to

45   biomass burning (BBOA) activities nearby. However, the BrC components responsible for light

46   absorption remain relatively unknown; this hinders a thorough understanding of the relationships

47   between optical properties and chemical characteristics and, in turn, the realization of a generalized

48   framework that can be extended to other sources and regions.

49   In this work, we present simultaneous measurements of aerosol chemical composition and light

50   absorption of aerosol particles at a suburban site downwind of Guangzhou in the PRD, China.

51   Contributions of BC and BrC to total aerosol light absorption were differentiated and quantified

52   using measurements from a seven-wavelength aethalometer. Sources of OA, which were

53   determined using PMF analysis, were correlated to BrC light absorption to identify the major

54   contributor(s) to short-wavelength light absorption. More detailed chemical characteristics, such

55   as N-containing ion fragments, the degree of unsaturation (indicated by the ion double bond

56   equivalent, or ion DBE), and the degree of oxygenation (indicated by the number of oxygen atoms

57   in ions), were also used to investigate the structural characteristics of BrC related to light

58   absorption.

59   Methodology

60   1. Sampling site

61   We conducted field measurements at the Guangzhou Panyu Atmospheric Composition Station

62   (GPACS, 23°00′ N, 113°21′ E), on the periphery of Guangzhou, China, from November 7, 2014

Atmospheric
Chemistry
and Physics
Discussions

63   to January 3, 2015. The GPACS is located on top of a hill with an altitude of approximately 150

64   m a.s.l. (Cheung et al., 2016; Tan et al., 2013; Zou et al., 2015); it is approximately 15 km south

65   of the city center and was downwind of the central city throughout the sampling period, during

66   which north winds prevailed (Qin et al., 2017).

67   2.   Measurements and data analysis

68   Aerosol light absorption was measured with a seven-wavelength aethalometer (Magee Scientific,

69   model AE33) at 370, 470, 520, 590, 660, 880, and 950 nm. Ambient air was drawn through a 2.5-

70   µm cut-off inlet at 2 L/min before entering the aethalometer; particles were collected on the filter

71   substrate, and light attenuation at the wavelengths above was recorded continuously. The optical

72   properties of the collected particles were determined by comparing light attenuation in particle-

73   laden and particle-free filter areas (Weingartner et al., 2003). To convert aerosol particles light

74   attenuation coefficients at the filter substrate to the light absorption coefficients suspended in the

75   air, a real-time compensation parameter k and a fixed multiple scattering parameter C were used.

76   The real-time loading effect correction was performed using two parallel measurements of optical

77   attenuations at different accumulation rates. C_{ref} =2.14 for quartz filter and C_{ref}=1.57 for

78   tetrafluoroethylene (TFE)-coated glass filter were recommended from previously studies for the

79   fresh soot particles (Drinovec et al., 2015; Weingartner et al., 2003). However, with the presence

80   of semi-volatile oxidation products, significantly higher values (C =3.6±0.6) were observed in the

81   organic coating experiment using a quartz filter (Weingartner et al., 2003). Wavelength

82   dependence of C has also been reported in the literature (Arnott et al., 2005; Schmid et al., 2006;

83   Segura et al., 2014) . A broad range of C (from 2.8 to 7.8) at several sites was also used by Collaud

84   Coen et al. (2010). As the multiple scattering parameter (C) may be site specific, we further

85   compared the absorption from AE33 with the co-located measurements. Here, we extracted the

86   light absorption based on extinction and scattering measurements from cavity ring-

87   down spectroscopy (CRD, Hexin XG-1000) and Nephelometer (TSI, 3563), respectively, as below.

88    $$b_{abs} = \sigma_{ext} - \sigma_{sp} \qquad (1)$$

89   where b_{abs}, σ_{ext} and σ_{sp} are absorption coefficient, extinction coefficient and scattering

90   coefficient.

91   The scatter plot of absorption at 532 nm from measurement from the aethalometer (AE33) and that

92   calculated from CRD and Nephelometer (CRD-Neph) is displayed in Figure 1. AE 33 absorption

Atmospheric
Chemistry
and Physics
Discussions

Open Access

EGU

93   coefficient was higher than the absorption estimated from Eq. 1. by a factor of 2.10. Therefore, the

94   final multiple scattering parameter (C) was set to $C_{final} = C_{ref} \times 2.10 = 3.29$. This value is

95   comparable with previous aethalometer measurements (C=3.48) in the PRD region (Wu et al.,

96   2009, 2013).

97   The non-refractory chemical composition of submicron aerosols was measured with an Aerodyne

98   HR-ToF-AMS (Aerodyne Research Inc., Billerica, MA, USA). Briefly, the AMS collected five-

99   minute-average particle mass spectra for the high-sensitivity V plus particle time-of-flight (PToF)

100   mode and the high-resolution W mode. AMS data analysis was performed using the SQUIRREL

101   (v1.56D) and PIKA (v1.15D) toolkits in Igor Pro (WaveMetrics Inc., Lake Oswego, OR). Source

102   apportionment was performed via PMF analysis with Multilinear Engine 2 (ME-2) via the SoFi

103   interface (Canonaco et al., 2013). Five factors, including HOA, COA, BBOA, semi-volatile

104   oxygenated organic aerosol (SVOOA), and low-volatility oxygenated organic aerosol (LVOOA),

105   were resolved (Qin et al., 2017). The campaign average OA composition was dominated by

106   surrogates of SOA (SVOOA + LVOOA). However, freshly-emitted hydrocarbon-like organic

107   aerosols (HOA) contributed up to 40.0% of OA during high-OA periods; during nighttime, HOA

108   contributed 23.8% to 28.4% on average. BBOA contributed 9.6% (1.87 µg/m^3) of total OA in

109   November and 6.5% (1.38 µg/m^3) in December. AMS data treatment was discussed in detail in

110   Qin et al. (2017). Data from a thermo-optical elemental carbon and organic carbon (ECOC)

111   analyzer (Sunset Laboratory Inc.) were also used for comparison.

112   Results and discussion

113   1. Aerosol absorption

114   Figure 2a shows the box-whisker plot of aerosol absorption coefficients (b_{abs}) from 370 nm to 950

115   nm from the aethalometer measurements during the campaign. The campaign-average absorption

116   coefficients were 56.00 Mm^{-1} at 370 nm, 40.99 Mm^{-1} at 470 nm, 34.76 Mm^{-1} at 520 nm, 29.91

117   Mm^{-1} at 590 nm, 26.69 Mm^{-1} at 660 nm, 18.06 Mm^{-1} at 880 nm, and 16.71 Mm^{-1} at 950 nm.

118   In multi-wavelength absorption measurements, the total absorption Ångström exponent (AAE) can

119   be calculated by a power-law fitting of the absorption coefficient over all available wavelengths.

120   AAE of unity has been widely used for pure black carbon, while a shift to higher AAE value has

121   been observed with the presence of brown carbon. The reason behind is that BrC has a much

122   stronger absorption at UV and short visible wavelengths than at long visible wavelengths, which

Atmospheric
Chemistry
and Physics
Discussions

123   yields a steeper curve (Andreae and Gelencsér, 2006; Bergstrom et al., 2007; Bond and Bergstrom,

124   2006). The presence of non-absorbing OA shells over BC cores may also lead to a shift of AAE

125   (Gyawali et al., 2009). This latter possibility is analyzed in a separated manuscript (Li et al., in

126   preparation). As shown in Figure 2b, the AAE values, which average at 1.43, are almost always

127   higher than 1, indicating appreciable contributions from BrC to particle light absorption at this site.

128

129   To further explore the importance of BrC at this site, BrC absorption at a short wavelength λ_1

130   ($b_{BrC,\lambda 1}$) can be derived by subtracting BC absorption ($b_{BC,\lambda 1}$) from the total aerosol absorption

131   (Lack and Langridge, 2013) via:

132    $$b_{BrC,\lambda 1} = b_{\lambda 1} - b_{BC,\lambda 1} \qquad (2)$$

133   where absorption $b_{\lambda 1}$ is the measured absorption at the short wavelength λ_1. BC absorption at λ_1

134   ($b_{BC,\lambda 1}$) can be obtained from the AAE value of BC (AAE_{BC}) via:

135

136    $$b_{BC,\lambda 1} = b_{\lambda 2} \times (\lambda_2 / \lambda_1)^{AAE_{BC}} \qquad (3)$$

137   where $b_{\lambda 2}$ is the absorption at a longer wavelength λ_2 (880 nm), which is assumed to have no

138   contributions from BrC or dust (Drinovec et al., 2015; Zhu et al., 2017). The uncertainty involved

139   in attributing BrC and BC absorption at short wavelengths has been explored explicitly by Lack

140   and Langridge (2013).

141   Figure 3 shows the b_{abs} attributed to BC and BrC (b_{BC} and b_{BrC}) at different wavelengths. Aerosol

142   light absorption coefficients were dominated by BC, but b_{BrC} was not negligible, especially at short

143   wavelengths. The campaign-average b_{BrC} values were 13.67, 7.56, 4.49, 3.22, and 2.81 Mm^{-1} at

144   370, 470, 520, 590, and 660 nm, respectively; BrC absorption contributed 23.6%, 18.1%, 10.7%,

145   10.7%, and 10.5% of the total absorption at the corresponding wavelengths. The proportions of

146   BrC and BC in our campaign were slightly higher than those reported an earlier study in the PRD

147   by Yuan et al. (2016). In their study, the average light absorption contributions of BrC during

148   Shenzhen winter, Shenzhen fall, and Heshan fall campaigns were 11.7%, 6.3%, and 12.1% at 405

149   nm and 10.0%, 4.1%, and 5.5% at 532 nm, respectively.

150   Figure 4 shows the diurnal variations of b_{BrC} at 370, 470, 520, 590, and 660 nm. At all wavelengths,

151   b_{BrC} was relatively constant from 00:00 LT to 16:00 LT, at which time it began to increase, peaking

Atmospheric
Chemistry
and Physics
Discussions

152   at 21:00 LT and then decreasing until 24:00 LT. These changes may be attributed to diurnal

153   changes in BrC sources, which most likely originated from crop residual burning in fall and winter

154   in nearby regions (Wang et al., 2017). The diurnal variations of the different wavelengths were not

155   significantly different, although short wavelengths exhibited more obvious diurnal variations.

156   2.   Correlation of light absorption by BrC with OA components

157   To explore the possible sources of BrC, correlations were determined between b_{BrC} at 370 nm

158   ($b_{BrC,370}$) and various OA types. Data at 370 nm were chosen (over data at longer wavelengths) for

159   their higher signal-to-noise ratios and larger contributions of BrC to light absorption. Figure 5

160   shows that BBOA concentrations and $b_{BrC,370}$ were well correlated (Pearson's correlation

161   coefficient, R_P = 0.58). More interestingly, a moderate correlation (R_p = 0.40) was also found

162   between $b_{BrC,370}$ and the LVOOA mass concentration. Although the LVOOA factor was not further

163   resolved into OOA factors with biomass origins, it is likely that a portion of LVOOA was formed

164   from biomass burning precursors through either gas-phase oxidation or heterogeneous reactions.

165   Satish et al. (2017) found correlations between BrC absorption and both primary BBOA and

166   BBOA-related SVOOA factors. They also reported that the slope of the correlation between

167    $b_{BrC,370}$ and BBOA (slope = 1.35) was 4.8 times higher than that between $b_{brc,370}$ and one of the

168   biomass burning SVOOA factors (slope = 0.28), indicating that aging may have reduced the

169   absorption capacity of biomass-related OA.

170   Multiple regression analysis was also used to resolve the correlation factors of each OA component

171   ($m^2\ g^{-1}$) at each wavelength.

172   b_{BrC}= a*[HOA]+b*[COA]+c*[BBOA]+d*[SVOOA]+e*[LVOOA]   (4)

173   where a, b, c, d, e indicates the correlation factors of each OA component ($m^2\ g^{-1}$) and [..] indicates

174   the mass concentration of each OA component. These correlation factors obtained are equivalent

175   to MAC mass absorption coefficient (MAC) of each OA component. We will use these factors to

176   compare with MAC reported in the literature later.

177   Washenfelder et al. (2015) reported a MAC of 1.3 ± 0.06 $m^2\ g^{-1}$ using the b_{BrC} at 365 nm for

178   BBOA in the rural southeastern United States, which was 40 to 135 times higher than the MAC

179   values reported for other OA factors. Di Lorenzo et al. (2017) found that both BBOA and more-

180   oxidized oxygenated organic aerosol (MO-OOA) were associated with water soluble BrC and that

Atmospheric
Chemistry
and Physics
Discussions

181 the MAC of BBOA doubled that of MO-OOA. However, Forrister et al. (2015) observed that BrC

182 in wildfire plumes had a lifetime of roughly 9 to 15 hours, probably due to conversion to SOA

183 with lower light absorption capacity. In our study, the MAC (correlation factor in Table 1) of

184 BBOA at 370 nm was 3.4 ± 0.41 m^2 g^{-1}, roughly 3.4 times that of LVOOA (1.04 ± 0.08 m^2 g^{-1}).

185 Like the studies listed above (Forrister et al., 2015; Di Lorenzo et al., 2017; Washenfelder et al.,

186 2015), our results suggest that the absorption coefficient of nascent BBOA is higher than that of

187 its aged counterpart at short wavelength. However, it should be noted that LVOOA might consist

188 of some other non-absorbing SOA components with no biomass origin. It is therefore important to

189 consider chromophore lifetimes when modeling light absorption by BrC. As noted in Laskin et al.

190 (2015), the physicochemical properties of chromophores in BrC may exhibit dynamic changes that

191 are not yet sufficiently understood. In addition, the difference between MAC values of BBOA and

192 LVOOA decreased for longer wavelengths. The MAC values of BBOA were roughly 3.4, 1.8, 1.5,

193 1.48, and 0.80 times those of LVOOA at 370, 470, 520, 570, and 660 nm, respectively.   The

194 contribution to total absorption coefficient also varied with wavelengths. The contribution from

195 BBOA decrease from 25.8% to 10.1% from 370 nm to 660 nm, while the contribution from

196 LVOOA increase from 49.3% to 60.2 % from 370nm to 660nm. The contribution of HOA was

197 more stable across different wavelengths but was also significant, likely due to the high mass

198 concentration of HOA. Altogether, these observations indicate that the wavelength-dependent light

199 absorption of different OAs must be considered in light absorption models.

200 3.   Correlation of b_{BrC} with N-containing organic ions

201 The chromophores in BrC that are responsible for OA light absorption are not well characterized.

202 Structurally, light absorption depends on the extent of sp^2 hybridization, in which π electrons are

203 usually found (Bond and Bergstrom, 2006). Of the elements commonly found in OA, both C and

204 N have strong tendencies toward sp^2 hybridization. It has also been found that, despite their small

205 OA mass fraction contributions, N-containing organic species in OA can be responsible for

206 appreciable light absorption (Chen et al., 2016; Laskin et al., 2015). Thus, we examined the

207 correlations between b_{BrC} and N-containing ions from AMS measurements. These ion fragments,

208 including the $C_xH_yN^+$ and $C_xH_yO_zN^+$ families, likely originated from N-heterocyclic compounds.

209 Figure 6 shows that the mass loadings of $C_xH_yN^+$ and $C_xH_yO_zN^{++}$ families are correlated with b_{BrC}

210 at 370 nm and that correlations are stronger for fragments containing both N and O atoms. These

211 results are consistent with Chen et al. (2016), who suggested that organic compounds with O and

Atmospheric
Chemistry
and Physics
Discussions

212   N atoms might contribute substantially to total light absorption and fluorescence in OA

213   components.

214   The effects of oxygenation (as indicated by the number of O atoms in an ion) and

215   unsaturation/cyclization (as indicated by the ion double bond equivalent, or ion DBE) were also

216   examined for each $C_xH_yN^+$ and $C_xH_yO_zN^+$ ion family. Several studies found that species with high

217   DBE values may have substantial network of conjugated double bonds and likely contribute to

218   light absorption (Budisulistiorini et al., 2017; Laskin et al., 2014; Lin et al., 2016). The ion DBE

219   represents the number of double bonds (unsaturation) or rings (cyclization) that an ion contains

220   and is calculated on the basis of the elemental formula via the following equation:

221   $$DBE = C + 1 - H/2 - X/2 + N/2 \qquad (4)$$

222   where C, H, X, and N are the number of carbon, hydrogen, halogen (Cl, Br, I, and F), and nitrogen

223   atoms present in the ion, respectively.

224   Figure 7a shows the correlation coefficients between $b_{BrC,370}$ and the mass loadings of each of the

225   $C_xH_yN^+$ family at different DBE values. For the C_xH_yN family, R_p increased as DBE increased

226   (except for ions with a DBE of 1), suggesting that $b_{BrC,370}$ was better correlated with fragments

227   with higher degrees of unsaturation or cyclization. Indeed, in saturated organics, light absorption

228   involves excitation of *n* electrons, which requires more energy and, therefore, shorter incident

229   wavelengths (e.g., short UV). In unsaturated organics, the delocalized π electrons in clusters of sp^2

230   hybrid bonds, as well as those in large conjugated systems, can extend absorption from short UV

231   to longer wavelengths into the near-visible spectrum. These structural features may explain in part

232   the increased correlation between mass loadings of the $C_xH_yN^+$ family and light absorption with

233   decreasing ion saturation. For the $C_xH_yO_zN^+$ family, we did not observe obvious trends in

234   correlation coefficient with changing degree of saturation/cyclization (Figure 7b). However, the

235   overall correlation was higher than those with $C_xH_yN^+$.

236   Conclusions

237   This paper presents collocated, real-time atmospheric particle light absorption and chemical

238   composition measurements at a suburban site in PRD, China. While BC dominated aerosol light

239   absorption, BrC also contributed to absorption at short wavelengths. The aerosol light absorption

240   coefficients of BrC were 13.67, 7.56, 4.49, 3.22, and 2.81 Mm^{-1} at 370, 470, 520, 590, and 660 nm,

241 respectively, and BrC contributed 23.6%, 18.1%, 10.7%, 10.7%, and 10.5% of the total absorption

242 at the corresponding wavelengths. Hydrocarbon-like organic aerosol (HOA), biomass burning

243 organic aerosol (BBOA) and low-volatility oxygenated organic aerosol (LVOOA) were also

244 substantial for the source of BrC. At short wavelength (370 nm), the mass absorption coefficient

245 of BBOA was higher than those of HOA and LVOOA. However, the difference between the mass

246 absorption coefficients of BBOA and other OA factors decreased with increasing wavelength. The

247 contribution of different OA sources to total absorption coefficient also varied with wavelengths.

248 Such a wavelength dependent trend is also observed for their contribution to total BrC absorption

249 coefficients. $C_xH_yN^+$ and $C_xH_yO_zN^+$, were likely the chromophores responsible for the observed

250 BrC light absorption. The mass loadings of $C_xH_yN^+$ and $C_xH_yO_zN^+$ ion families became better

251 correlated with the BrC light absorption coefficient as their degrees of unsaturation/cyclization and

252 oxygenation increased. This study shows wavelength-dependent light absorption by BrC is

253 strongly influenced by moderately specific molecular characteristics such as degrees of

254 unsaturation/ cyclization and oxygenation. An exploration of the absorptive properties of more

255 specific molecular features, such as the chemical identities of BrC constituents, would require a

256 more detailed chemical characterization of the highly complex OA composition.

257

Acknowledgements

266

267

Atmospheric
Chemistry
and Physics
Discussions

References

268

269 Andreae, M. O. and Gelencsér, A.: Black carbon or brown carbon? The nature of light-absorbing
270 carbonaceous aerosols, Atmos. Chem. Phys., 6(3), 3419–3463, doi:10.5194/acpd-6-3419-2006,
271 2006.

272 Arnott, W. P., Hamasha, K., Moosmüller, H., Sheridan, P. J. and Ogren, J. A.: Towards aerosol
273 light-absorption measurements with a 7-wavelength aethalometer: Evaluation with a
274 photoacoustic instrument and 3-wavelength nephelometer, Aerosol Sci. Technol., 39(1), 17–29,
275 doi:10.1080/027868290901972, 2005.

276 Bergstrom, R. W., Pilewskie, P., Russell, P. B., Redemann, J., Bond, T. C., Quinn, P. K. and
277 Sierau, B.: Spectral absorption properties of atmospheric aerosols, Atmos. Chem. Phys., 7(23),
278 5937–5943, doi:10.5194/acp-7-5937-2007, 2007.

279 Bond, T. C. and Bergstrom, R. W.: Light Absorption by Carbonaceous Particles: An
280 Investigative Review, Aerosol Sci. Technol., 40(1), 27–67, doi:10.1080/02786820500421521,
281 2006.

282 Budisulistiorini, S. H., Riva, M., Williams, M., Chen, J., Itoh, M., Surratt, J. D. and Kuwata, M.:
283 Light-Absorbing Brown Carbon Aerosol Constituents from Combustion of Indonesian Peat and
284 Biomass, Environ. Sci. Technol., 51(8), 4415–4423, doi:10.1021/acs.est.7b00397, 2017.

285 Canonaco, F., Crippa, M., Slowik, J. G., Baltensperger, U. and Prévôt, A. S. H.: SoFi, an IGOR-
286 based interface for the efficient use of the generalized multilinear engine (ME-2) for the source
287 apportionment: ME-2 application to aerosol mass spectrometer data, Atmos. Meas. Tech., 6(12),
288 3649–3661, doi:10.5194/amt-6-3649-2013, 2013.

289 Chan, C. K. and Yao, X.: Air pollution in mega cities in China, Atmos. Environ., 42(1), 1–42,
290 doi:10.1016/j.atmosenv.2007.09.003, 2008.

291 Chen, Q., Ikemori, F. and Mochida, M.: Light Absorption and Excitation-Emission Fluorescence
292 of Urban Organic Aerosol Components and Their Relationship to Chemical Structure, Environ.
293 Sci. Technol., 50(20), 10859–10868, doi:10.1021/acs.est.6b02541, 2016.

294 Cheung, H. H. Y., Tan, H., Xu, H., Li, F., Wu, C., Yu, J. Z. and Chan, C. K.: Measurements of
295 non-volatile aerosols with a VTDMA and their correlations with carbonaceous aerosols in
296 Guangzhou, China, Atmos. Chem. Phys., 16(13), 8431–8446, doi:10.5194/acp-16-8431-2016,
297 2016.

298 Collaud Coen, M., Weingartner, E., Apituley, A., Ceburnis, D., Fierz-Schmidhauser, R., Flentje,
299 H., Henzing, J. S., Jennings, S. G., Moerman, M., Petzold, A., Schmid, O. and Baltensperger, U.:
300 Minimizing light absorption measurement artifacts of the Aethalometer: Evaluation of five
301 correction algorithms, Atmos. Meas. Tech., 3(2), 457–474, doi:10.5194/amt-3-457-2010, 2010.

302 Drinovec, L., Močnik, G., Zotter, P., Prévôt, A. S. H., Ruckstuhl, C., Coz, E., Rupakheti, M.,
303 Sciare, J., Müller, T., Wiedensohler, A. and Hansen, A. D. A.: The "dual-spot" Aethalometer: An
304 improved measurement of aerosol black carbon with real-time loading compensation, Atmos.
305 Meas. Tech., 8(5), 1965–1979, doi:10.5194/amt-8-1965-2015, 2015.

306 Feng, Y., Ramanathan, V. and Kotamarthi, V. R.: Brown carbon: A significant atmospheric

307   absorber of solar radiation, Atmos. Chem. Phys., 13(17), 8607–8621, doi:10.5194/acp-13-8607-
308   2013, 2013.

309   Forrister, H., Liu, J., Scheuer, E., Dibb, J., Ziemba, L., Thornhill, K. L., Anderson, B., Diskin,
310   G., Perring, A. E., Schwarz, J. P., Campuzano-Jost, P., Day, D. A., Palm, B. B., Jimenez, J. L.,
311   Nenes, A. and Weber, R. J.: Evolution of brown carbon in wildfire plumes, Geophys. Res. Lett.,
312   42(11), 4623–4630, doi:10.1002/2015GL063897, 2015.

313   Gen, M., Huang, D. and Chan, C. K.: Reactive uptake of glyoxal by ammonium containing salt
314   particles as a function of relative humidity, Environ. Sci. Technol., 52, 6903–6911,
315   doi:10.1021/acs.est.8b00606, 2018.

316   Gong, Z., Lan, Z., Xue, L., Zeng, L., He, L. and Huang, X.: Characterization of submicron
317   aerosols in the urban outflow of the central Pearl River Delta region of China, Front. Environ.
318   Sci. Eng. China, 6(5), 725–733, doi:10.1007/s11783-012-0441-8, 2012.

319   Gyawali, M., Arnott, W. P., Lewis, K. and Moosmüller, H.: In situ aerosol optics in Reno, NV,
320   USA during and after the summer 2008 California wildfires and the influence of aerosol
321   coatings, Atmos. Chem. Phys. Discuss., 9, 8007–8015, doi:10.5194/acp-9-8007-2009, 2009.

322   He, L.-Y., Huang, X.-F., Xue, L., Hu, M., Lin, Y., Zheng, J., Zhang, R. and Zhang, Y.-H.:
323   Submicron aerosol analysis and organic source apportionment in an urban atmosphere in Pearl
324   River Delta of China using high-resolution aerosol mass spectrometry, J. Geophys. Res.,
325   116(D12), D12304, doi:10.1029/2010JD014566, 2011.

326   Huang, X.-F. F., He, L.-Y. Y., Hu, M., Canagaratna, M. R., Kroll, J. H., Ng, N. L., Zhang, Y.-H.
327   H., Lin, Y., Xue, L., Sun, T.-L. L., Liu, X.-G. G., Shao, M., Jayne, J. T. and Worsnop, D. R.:
328   Characterization of submicron aerosols at a rural site in Pearl River Delta of China using an
329   Aerodyne High-Resolution Aerosol Mass Spectrometer, Atmos. Chem. Phys., 11(5), 1865–1877,
330   doi:10.5194/acp-11-1865-2011, 2011.

331   Lack, D. A. and Langridge, J. M.: On the attribution of black and brown carbon light absorption
332   using the angstrom exponent, Atmos. Chem. Phys., 13(20), 10535–10543, doi:10.5194/acp-13-
333   10535-2013, 2013.

334   Laskin, A., Laskin, J. and Nizkorodov, S. a.: Chemistry of Atmospheric Brown Carbon, Chem.
335   Rev., 115(10), 4335–4382, doi:10.1021/cr5006167, 2015.

336   Laskin, J., Laskin, A., Roach, P. J., Slysz, G. W., Anderson, G. A., Nizkorodov, S. A., Bones, D.
337   L. and Nguyen, L. Q.: Mass Spectrometry for Chemical Characterization of Organic Aerosols, ,
338   82(5), 2048–2058, doi:10.1029/2007JD008683, 2010.

339   Laskin, J., Laskin, A., Nizkorodov, S. A., Roach, P., Eckert, P., Gilles, M. K., Wang, B., Ji, H.,
340   Lee, J. and Hu, Q.: Molecular Selectivity of Brown Carbon Chromophores, 2014.

341   Li, Y. J., Sun, Y., Zhang, Q., Li, X., Li, M., Zhou, Z. and Chan, C. K.: Real-time chemical
342   characterization of atmospheric particulate matter in China : A review, Atmos. Environ., 158,
343   270–304, doi:10.1016/j.atmosenv.2017.02.027, 2017.

344   Lin, P., Aiona, P. K., Li, Y., Shiraiwa, M., Laskin, J., Nizkorodov, S. A. and Laskin, A.:
345   Molecular Characterization of Brown Carbon in Biomass Burning Aerosol Particles, Environ.
346   Sci. Technol., 50(21), 11815–11824, doi:10.1021/acs.est.6b03024, 2016.

Atmospheric
Chemistry
and Physics
Discussions

347   Liu, P. F., Abdelmalki, N., Hung, H. M., Wang, Y., Brune, W. H. and Martin, S. T.: Ultraviolet
348   and visible complex refractive indices of secondary organic material produced by photooxidation
349   of the aromatic compounds toluene and m-xylene, Atmos. Chem. Phys., 15(3), 1435–1446,
350   doi:10.5194/acp-15-1435-2015, 2015.

351   Di Lorenzo, R. A., Washenfelder, R. A., Attwood, A. R., Guo, H., Xu, L., Ng, N. L., Weber, R.
352   J., Baumann, K., Edgerton, E. and Young, C. J.: Molecular-Size-Separated Brown Carbon
353   Absorption for Biomass-Burning Aerosol at Multiple Field Sites, Environ. Sci. Technol., 51(6),
354   3128–3137, doi:10.1021/acs.est.6b06160, 2017.

355   Massabo, D., Caponi, L., Bernardoni, V., Bove, M. C., Brotto, P., Calzolai, G., Cassola, F.,
356   Chiari, M., Fedi, M. E., Fermo, P., Giannoni, M., Lucarelli, F., Nava, S., Piazzalunga, A., Valli,
357   G., Vecchi, R. and Prati, P.: Multi-wavelength optical determination of black and brown carbon
358   in atmospheric aerosols, Atmos. Environ., 108, 1–12, doi:10.1016/j.atmosenv.2015.02.058,
359   2015.

360   Qin, Y. M., Tan, H. B., Li, Y. J., Schurman, M. I., Li, F., Canonaco, F., Prévôt, A. S. H. and
361   Chan, C. K.: Impacts of traffic emissions on atmospheric particulate nitrate and organics at a
362   downwind site on the periphery of Guangzhou, China, Atmos. Chem. Phys., 2017(x), 1–31,
363   doi:10.5194/acp-2017-116, 2017.

364   Rinco, A. G., Guzma, M. I., Hoffmann, M. R. and Colussi, A. J.: Optical Absorptivity versus
365   Molecular Composition of Model Organic Aerosol Matter, , 10512–10520, 2009.

366   Satish, R., Shamjad, P., Thamban, N., Tripathi, S. and Rastogi, N.: Temporal Characteristics of
367   Brown Carbon over the Central Indo- Gangetic Plain, , doi:10.1021/acs.est.7b00734, 2017.

368   Schmid, O., Artaxo, P., Arnott, W. P., Chand, D., Gatti, L. V., Frank, G. P., Hoffer, A.,
369   Schnaiter, M. and Andreae, M. O.: Spectral light absorption by ambient aerosols influenced by
370   biomass burning in the Amazon Basin. I: Comparison and field calibration of absorption
371   measurement techniques, Atmos. Chem. Phys., 6(11), 3443–3462, doi:10.5194/acp-6-3443-2006,
372   2006.

373   Segura, S., Estellés, V., Titos, G., Lyamani, H., Utrillas, M. P., Zotter, P., Prévôt, A. S. H.,
374   Močnik, G., Alados-Arboledas, L. and Martínez-Lozano, J. A.: Determination and analysis of in
375   situ spectral aerosol optical properties by a multi-instrumental approach, Atmos. Meas. Tech.,
376   7(8), 2373–2387, doi:10.5194/amt-7-2373-2014, 2014.

377   Sun, H., Biedermann, L. and Bond, T. C.: Color of brown carbon : A model for ultraviolet and
378   visible light absorption by organic carbon aerosol, , 34(August), 1–5,
379   doi:10.1029/2007GL029797, 2007.

380   Tan, H., Yin, Y., Gu, X., Li, F., Chan, P. W., Xu, H., Deng, X. and Wan, Q.: An observational
381   study of the hygroscopic properties of aerosols over the Pearl River Delta region, Atmos.
382   Environ., 77, 817–826, doi:10.1016/j.atmosenv.2013.05.049, 2013.

383   Wang, Y., Hu, M., Lin, P., Guo, Q., Wu, Z., Li, M., Zeng, L., Song, Y., Zeng, L., Wu, Y., Guo,
384   S., Huang, X. and He, L.: Molecular Characterization of Nitrogen-Containing Organic
385   Compounds in Humic-like Substances Emitted from Straw Residue Burning, Environ. Sci.
386   Technol., 51(11), 5951–5961, doi:10.1021/acs.est.7b00248, 2017.

387   Washenfelder, R. A., Attwood, A. R., Brock, C. A., Guo, H., Xu, L., Weber, R. J., Ng, N. L.,
388   Allen, H. M., Ayres, B. R., Baumann, K., Cohen, R. C., Draper, D. C., Duffey, K. C., Edgerton,
389   E., Fry, J. L., Hu, W. W., Jimenez, J. L., Palm, B. B., Romer, P., Stone, E. A., Wooldridge, P. J.
390   and Brown, S. S.: Biomass burning dominates brown carbon absorption in the rural southeastern
391   United States, Geophys. Res. Lett., 42(2), 653–664, doi:10.1002/2014GL062444, 2015.

392   Weingartner, E., Saathoff, H., Schnaiter, M., Streit, N., Bitnar, B. and Baltensperger, U.:
393   Absorption of light by soot particles: Determination of the absorption coefficient by means of
394   aethalometers, J. Aerosol Sci., 34(10), 1445–1463, doi:10.1016/S0021-8502(03)00359-8, 2003.

395   Wu, D., Mao, J. T., Deng, X. J., Tie, X. X., Zhang, Y. H., Zeng, L. M., Li, F., Tan, H. B., Bi, X.
396   Y., Huang, X. Y., Chen, J. and Deng, T.: Black carbon aerosols and their radiative properties in
397   the Pearl River Delta region, Sci. China, Ser. D Earth Sci., 52(8), 1152–1163,
398   doi:10.1007/s11430-009-0115-y, 2009.

399   Wu, D., Wu, C., Liao, B., Chen, H., Wu, M., Li, F., Tan, H., Deng, T., Li, H., Jiang, D. and Yu,
400   J. Z.: Black carbon over the South China Sea and in various continental locations in South China,
401   Atmos. Chem. Phys., 13(24), 12257–12270, doi:10.5194/acp-13-12257-2013, 2013.

402   Yan, C., Zheng, M., Bosch, C., Andersson, A., Desyaterik, Y., Sullivan, A. P., Collett, J. L.,
403   Zhao, B., Wang, S., He, K. and Gustafsson, Ö.: Important fossil source contribution to brown
404   carbon in Beijing during winter, Nat. Publ. Gr., 1–10, doi:10.1038/srep43182, 2017.

405   Yuan, J. F., Huang, X. F., Cao, L. M., Cui, J., Zhu, Q., Huang, C. N., Lan, Z. J. and He, L. Y.:
406   Light absorption of brown carbon aerosol in the PRD region of China, Atmos. Chem. Phys.,
407   16(3), 1433–1443, doi:10.5194/acp-16-1433-2016, 2016.

408   Zhu, C.-S., Cao, J.-J., Hu, T.-F., Shen, Z.-X., Tie, X.-X., Huang, H., Wang, Q.-Y., Huang, R.-J.,
409   Zhao, Z.-Z., Močnik, G. and Hansen, A. D. A.: Spectral dependence of aerosol light absorption
410   at an urban and a remote site over the Tibetan Plateau, Sci. Total Environ., 590–591(97), 14–21,
411   doi:10.1016/j.scitotenv.2017.03.057, 2017.

412   Zou, Y., Deng, X. J., Zhu, D., Gong, D. C., Wang, H., Li, F., Tan, H. B., Deng, T., Mai, B. R.,
413   Liu, X. T. and Wang, B. G.: Characteristics of 1 year of observational data of VOCs, NO_x and O_3
414   at a suburban site in Guangzhou, China, Atmos. Chem. Phys., 15(12), 6625–6636,
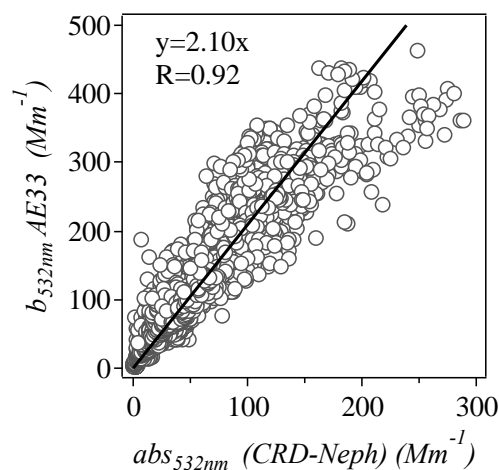415   doi:10.5194/acp-15-6625-2015, 2015.

416

417   Table

418   Table 1. Multilinear regression analyses between b_{BrC} at each wavelength and mass loading of

419   different OA factors from AMS-PMF/ME-2.

	370 nm		470 nm		520 nm		590 nm		660 nm	
	Correlation factor ($m^2\,g^{-1}$)	Contribution to b_{BrC}	Correlation factor ($m^2\,g^{-1}$)	Contribution to b_{BrC}	Correlation factor ($m^2\,g^{-1}$)	Contribution to b_{BrC}	Correlation factor ($m^2\,g^{-1}$)	Contribution to b_{BrC}	Correlation factor ($m^2\,g^{-1}$)	Contribution to b_{BrC}
HOA	0.61 ± 0.05	22.7%	0.38 ± 0.03	25.4%	0.22 ± 0.02	24.5%	0.16 ± 0.02	25.1%	0.16 ± 0.01	27.9%
BBOA	3.4 ± 0.41	25.2%	1.2 ± 0.26	15.9%	0.63 ± 0.18	13.9%	0.43 ± 0.14	13.4%	0.21 ± 0.11	10.3%
LVOOA	1.04 ± 0.08	52.2%	0.65 ± 0.05	58.7%	0.41 ± 0.04	61.5%	0.29 ± 0.03	61.5%	0.26 ± 0.02	61.3%

420

421   Notes: 1) Correlation coefficient (R) for each regression analysis: 0.65 at 370 nm, 0.58 at 470 nm, 0.51 at 520 nm,

422   0.51 at 570 nm and 0.54 at 660 nm; 2) The correlation factors for COA and SVOOA are near zero at all wavelength,

423   indicating a negligible contribution from these factors. So only the correlation factors for HOA, BBOA and LVOOA

424   are listed in the table

425

426

427   Figures

428

429   Figure 1. Scatter plot of absorption coefficients at 532 nm measured with aethalometer (AE33)

430   and those estimated from cavity ring-down spectroscopy (CRD) and Nephelometer measurements.
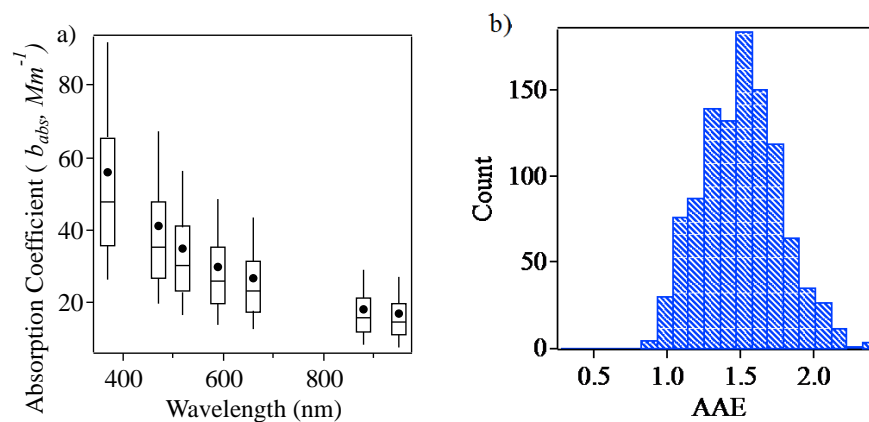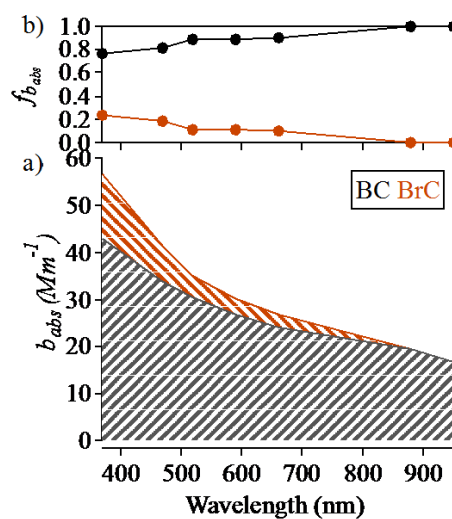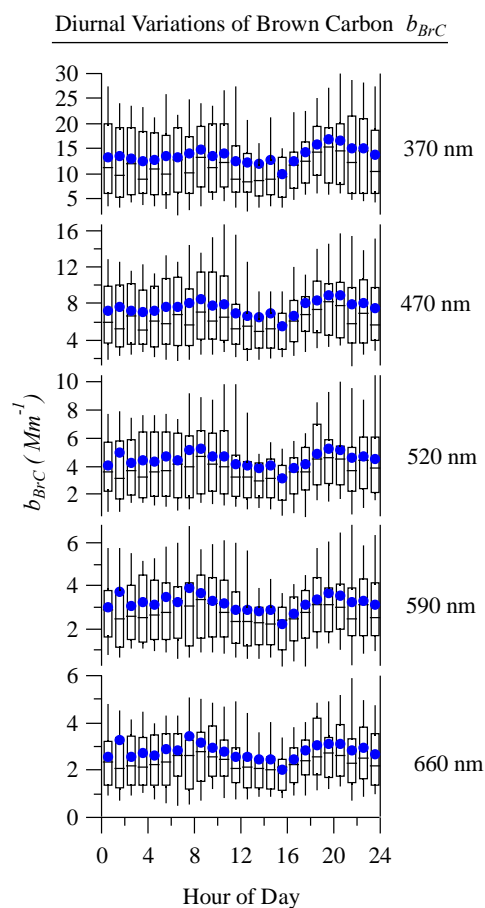
431

432

433   Figure 2. a) Box-whisker plot of absorption coefficient at seven wavelengths as measured with
434   the AE33; b) Histogram of AAE values over the measurement campaign.

435

436

Figure 3. a) Fractions of BC and BrC contributions to aerosol particle light absorption at different

wavelengths; b) Contributions of BC and BrC to the total light absorption coefficient at different

wavelengths.

440

Atmospheric
Chemistry
and Physics
Discussions

Open Access

441

442   Figure 4. Diurnal variations of BrC light absorption coefficients (b_{BrC}) at different wavelengths.
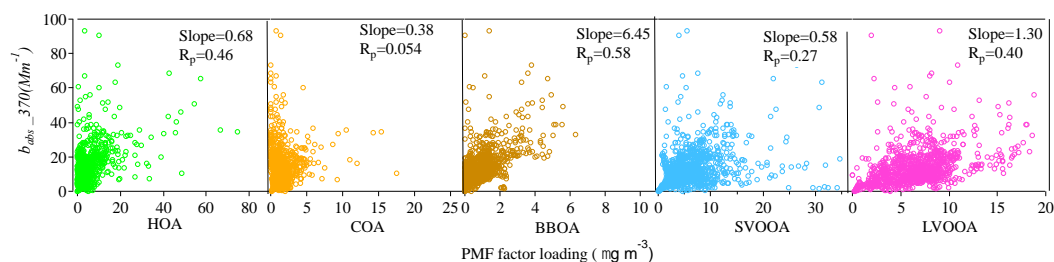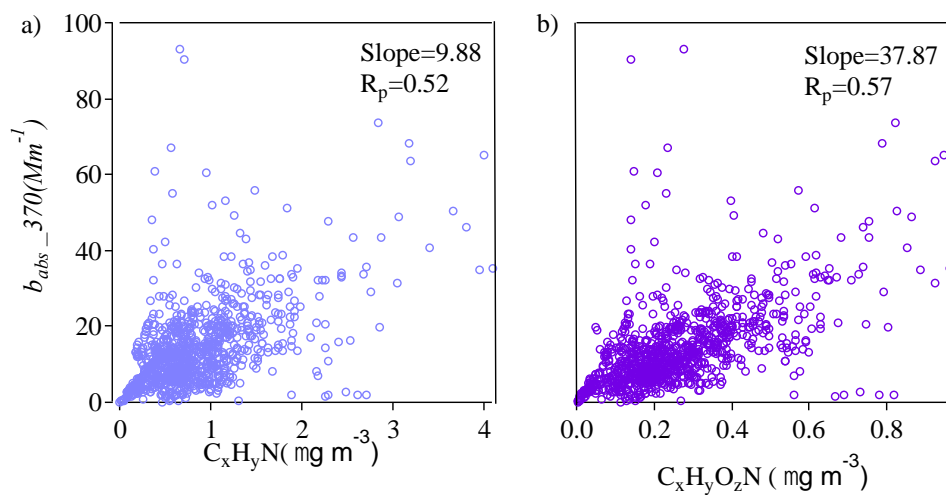
443

444

445

Figure 5. Correlations between the BrC absorption coefficients at 370 nm and the mass loadings of OA factors resolved by AMS-PMF/ME-2.

448

449
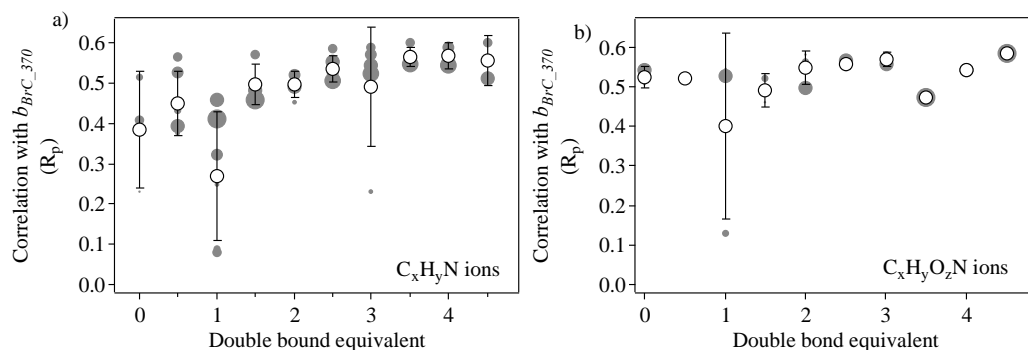
450

451

Figure 6. Correlations between BrC absorption coefficients at 370 nm and mass concentrations of

N-containing organic ion families.

454

455

456   Figure 7. Correlation coefficients between BrC absorption coefficient at 370 nm and N-containing

457   organic ion fragments grouped by double bond equivalence (panels a and b) and number of oxygen

458   atoms (panel c). Larger grey dots correspond to higher carbon numbers.